Volume 140 | Number 2 | 21 January 2015 | Pages 373–672

Analyst

www.rsc.org/analyst

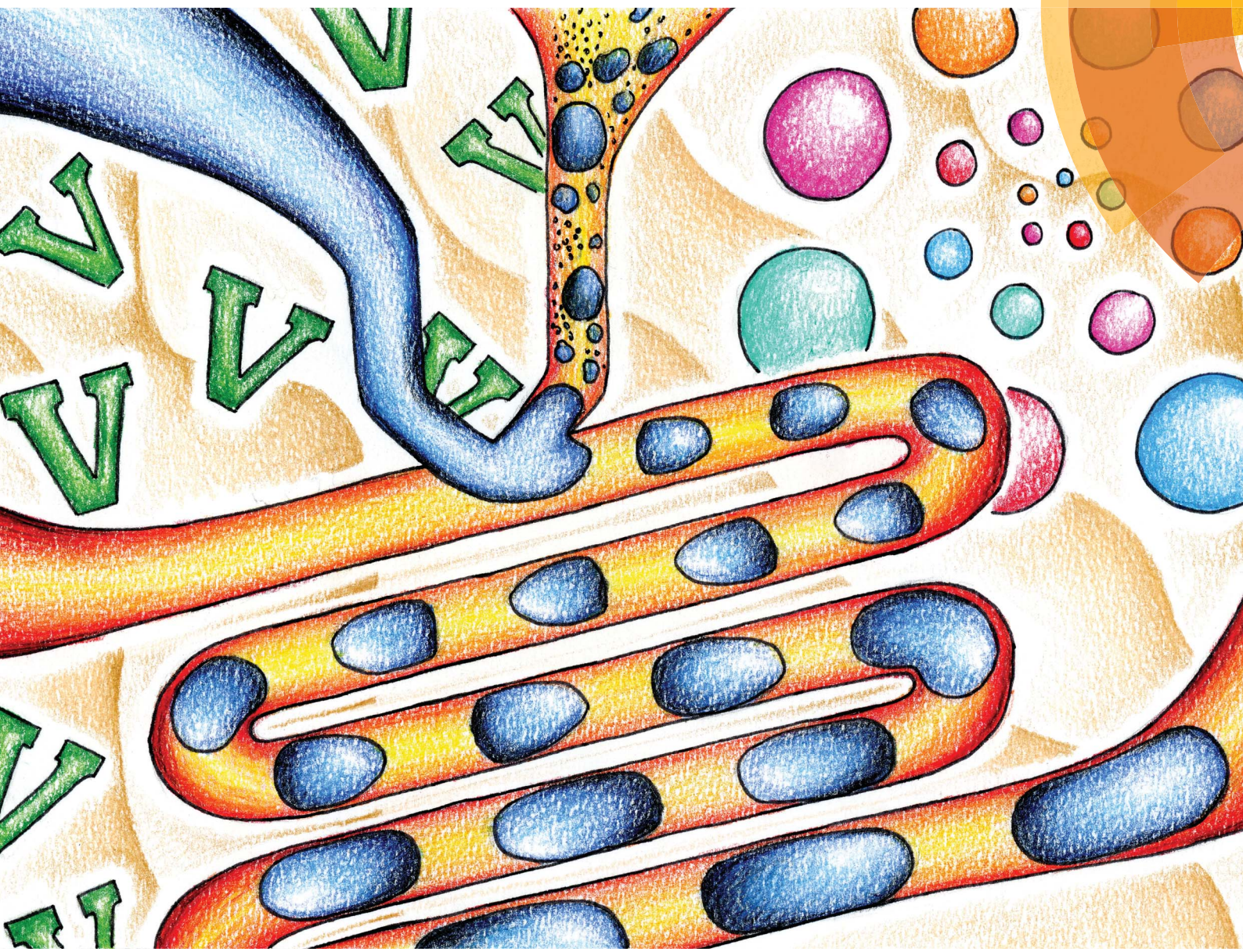

ISSN 0003-2654

ROYAL SOCIETY OF CHEMISTRY

PAPER
Andrew deMello *et al.*
"V-junction": a novel structure for high-speed generation of bespoke droplet flows

Analyst

PAPER

View Article Online
View Journal | View Issue

Cite this: *Analyst*, 2015, **140**, 414

"V-junction": a novel structure for high-speed generation of bespoke droplet flows†

Yun Ding, Xavier Casadevall i Solvas and Andrew deMello*

We present the use of microfluidic "V-junctions" as a droplet generation strategy that incorporates enhanced performance characteristics when compared to more traditional "T-junction" formats. This includes the ability to generate target-sized droplets from the very first one, efficient switching between multiple input samples, the production of a wide range of droplet sizes (and size gradients) and the facile generation of droplets with residence time gradients. Additionally, the use of V-junction droplet generators enables the suspension and subsequent resumption of droplet flows at times defined by the user. The high degree of operational flexibility allows a wide range of droplet sizes, payloads, spacings and generation frequencies to be obtained, which in turn provides for an enhanced design space for droplet-based experimentation. We show that the V-junction retains the simplicity of operation associated with T-junction formats, whilst offering functionalities normally associated with droplet-on-demand technologies.

Received 23rd September 2014
Accepted 20th October 2014

DOI: 10.1039/c4an01730g

www.rsc.org/analyst

Introduction

Microfluidic technologies have engendered many new and exciting opportunities within the chemical and biological sciences. They provide for high analytical efficiency and throughput, and harness the dependency of fluid-flow on scale to empower new experimental formats (such as digital PCR and single cell-based screens).[1–3] This is possible due to reduced sample and reagent consumption, efficient mass and thermal transport (due to smaller volumes) and exquisite ability to integrate a range of functional components.[4–7] In recent years, droplet-based (or segmented-flow) microfluidic systems have been used to great effect in performing high-throughput and high-efficiency chemical and biological assays. Sub-nanoliter droplets may be generated at high speeds (kHz rates), with their size and chemical payloads being controlled in a reproducible manner. Each droplet acts as an individual compartment that isolates and protects its contents from microchannel surfaces and cross-contamination between adjacent samples.[8,9] Over a decade has passed since Thorsen *et al.*[10] and Anna *et al.*[11] first demonstrated highly monodisperse droplet formation using the T-junction and flow focusing strategies and in that time a diversity of functional components have been developed to process such droplet flows. These include elegant tools for droplet immobilization, mixing, incubation, dosing, merging, splitting, diluting and sorting.[12–19] Accordingly, droplet-based microfluidic platforms have rapidly been adopted as powerful research tools in many chemical and biological laboratories. As such, an increasing number of "non-microfluidic" researchers are becoming interested in applying these technologies to address specific chemical or biological problems, but are often reluctant to fully embrace them due to their complexity and high instrumental investment thresholds. Therefore, direct strategies that require simple basic equipment are highly desirable for performing droplet-based experiments. Indeed, in an ideal world, an experimental process would be hardcoded into the microfluidic device through geometric design and control of the physicochemical properties such as hydrodynamic resistances, surface properties, diffusion, solubility and chemical activity of the contained reagents.[19–23] In such a situation, the user would simply introduce the desired sample and the experiment would then "run itself".

Although numerous functions and droplet manipulations have been achieved through the use of passive microfluidic systems, there remain some key challenges that must be addressed prior to the realization of autonomous operation. Of special relevance is adoption of a droplet generation strategy that guarantees stable production of droplets with the desired size, frequency and spacing. Although formats for droplet generation are well-known, formation of bubbles at the beginning of an experiment or droplet generation at the wrong time (such as during initial unsteady transitory phases[15] or when asynchronous trains of droplets are produced)[20] are often terminal for experiment progress. Currently, there is no strategy that allows passive droplet generation whilst eliminating or preventing the formation of rogue droplets or bubbles. Conventional droplet generators, based on the T-junction and

Department of Chemistry and Applied Biosciences, Institute for Chemical and Bioengineering, ETH Zurich, Vladimir-Prelog-Weg 1, Zurich, 8093, Switzerland. E-mail: andrew.demello@chem.ethz.ch

† Electronic supplementary information (ESI) available. See DOI: 10.1039/c4an01730g

flow focusing formats, benefit from operational simplicity but suffer from the above problems, thus impacting experimental reproducibility.[24,25] To date, these issues have been resolved by adopting droplet-on-demand technologies,[26–28] which commonly involve the use of elaborate microvalves within channel gates or mechanical actuators to allow control of the droplet generation process. These methods typically require complex fabrication procedures and necessitate development of custom actuation and control algorithms. It should also be noted that droplet-on-demand operation has been realized through the adoption of complex, off-chip robotic solutions.[29] Herein, we present a modification of the traditional T-junction design, which we termed as the V-junction (Fig. 1a). The V-junction allows the generation of controllable droplet streams (from the first to the last) and requires only basic fabrication and manipulation techniques. By simply incorporating an additional side (or control) channel (Fig. 1a–3) at the junction, the generation of droplets is easily achieved and is additionally accompanied by several attractive features. These include the prevention of unwanted droplet generation, clean switching between multiple input samples, production of a large range of droplet sizes (and size gradients) and generation of droplet streams with residence time gradients. It is important to note that a structurally similar design (termed as K-junction) was introduced by Lin and co-workers.[30] This was used for the on-demand generation of cell encapsulating droplets using the assistance of an integrated pneumatic micropump. In comparison, we report for the first time a passive droplet generation system that fills in the gap between high-end (but complex) droplet-on-demand systems and simple/passive (but utility-limited) droplet generation methods.

Methods

Polydimethylsiloxane (PDMS) devices were fabricated using SU-8 master moulds and standard soft-lithographic methods.[31] After degassing and casting over an SU-8 master, PDMS (Sylgard 184, Dow Corning, USA) was oven-cured at 70 °C for 2 hours. The structured PDMS layer was then peeled off the master and sealed onto a flat (unstructured) PDMS layer by plasma bonding. Subsequently, the chip was kept overnight at 70 °C to firm the bond and to allow channel walls to recover their inherent hydrophobic surface properties.[32] During droplet-generation experiments, the entire microfluidic device was held on a glass slide (Thermo Scientific, Germany) and imaged under a microscope (Eclipse Ti-E, Nikon, Japan) using a high-speed camera (MotionPro Y5, IDT, UK). Fig. 1a illustrates the basic microfluidic structure, with all channels being 50 μm high. The main channel used to infuse the carrier phase (typically oil) and generate the segmented flow has a width of 100 μm. Side channels for discrete phase (typically water) infusion and droplet control (labelled 2 and 3, respectively) are divided in two segments: the top section being 100 μm wide and the lower section being 50 μm wide. The angle between the side channels is 60°, with the bisector perpendicular to the main channel. It should be noted that three sets of devices, with 30, 60° and 90° angles, were designed and tested (Fig. S1†). It was observed that a 60° angle provided for the best control capability.

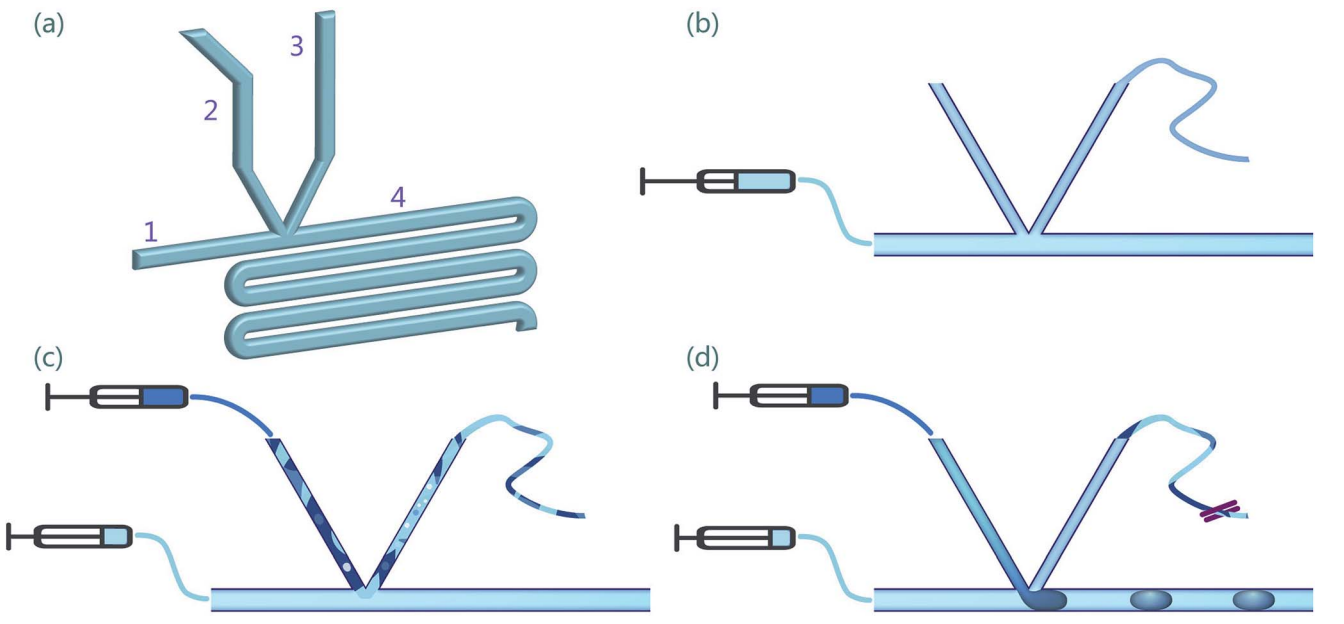

Fig. 1 (a) Schematic of the V-junction structure containing an oil inlet (1), a side channel (2) for water introduction, a side channel (3) for control, and a main channel and an observation zone (4). In the current design all channels are 50 μm in height. The angle between the two side channels is 60°. (b–d) Schematic illustration of chip operation. (b) A 30 cm long control-tubing is connected at the end of channel 3, all the systems are filled with oil. (c) *Open-mode*: with oil continuously being infused, the water phase begins to enter channel 2. Air bubbles, transitional emulsions and water are drained through channel 3. (d) *Closed-mode*: once impurities have been completely removed, the control-tubing is blocked and water enters the main channel forming stable droplets.

Mineral oil (Sigma-Aldrich, light oil form, 0.84 g ml^{-1}, UK) and deionized water (containing blue ink in some experiments) were used to create droplet streams. 5 wt% Span 80 (Sigma-Aldrich, UK) was added as a surfactant into mineral oil to stabilize droplets after formation. The oil–surfactant mixture was vortexed and degassed before use and syringe pumps (neMESYS Low Pressure Dosing Module, Cetoni, Germany) used to inject oil and water phases into the microchannels.

Unless otherwise indicated, droplet analysis was accomplished using ImageJ (v1.47, NIH, Bethesda, Maryland, USA) and Droplet Morphometry and Velocimetry software (DMV).[33]

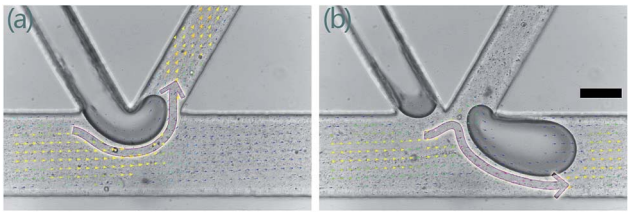

Fig. 2 PIV analysis of the two basic operation modes. The speed and direction of oil flow are indicated with arrows. (a) In *open-mode*, the oil flow goes into both the main channel and the side channel. A barrier flow by oil (marked with a hollow pink arrow) prevents the water phase from entering the main channel. (b) In *closed-mode*, no net flow occurs in the control channel. The oil phase creates droplets at the main channel by shearing in the water phase. Video for both cases is provided in the ESI, Video S2.† The scale bar is 50 μm.

Results and discussion

Binary mode: a world-to-chip interface that prevents unsolicited droplet introduction

The initial capabilities of the V-junction are first presented by applying two operational modes on the control channel: '*open*' or '*closed*'. These modes allow the dispersed phase (water in the current experiments) to either enter the main channel (*closed-mode*) or the control channel (*open-mode*). Fig. 1 illustrates a schematic of the set up for each mode of operation. It is noted that a length (30 cm) of soft tubing (TYGON ND 100-80 Tubing, ID 0.020 inches, OD 0.040 inches, USA) is connected to the exit of the control channel. Before starting an experiment (Fig. 1b), only the oil inlet (1) and control channel (3) are connected to the tubing. The device is first primed by pumping oil throughout the whole system, including the control-tubing. This step ensures that residual air (which is compressible) in the control-tubing is removed, and also aids in building a pressure balance during the initial state. While oil is continuously pumped at the desired flow-rate, the water inlet is then connected to the tubing to allow infusion of water into the system. During *open-mode* operation, all the fluids from the water inlet are directly eliminated through the control channel, including transitional air bubbles, oil, water and transient droplets. For the current device and an oil influx of 2 μl min^{-1}, the volumetric flow rate of water is maintained below 6 μl min^{-1} (although this still works for flow rates as high as 11 μl min^{-1}, Fig. S3†). Switching to *closed-mode* is simply achieved by closing the tubing of the control channel. As soon as the flow in the control channel stops, water enters the main channel and droplets are generated. Thereupon, the system functions as a T-junction (with improvements that will be discussed in the next section).

To better understand the transition between the *open* and *closed* modes, profiles of the oil flow for both modes of operation were visualized using Particle Image Velocimetry (PIV),[34] by seeding a small number (0.1 wt%) of polystyrene microspheres (5 μm diameter in aqueous suspensions, Sigma-Aldrich, Switzerland) into the oil phase. The results of the PIV analysis are shown in Fig. 2 and Video S2.† In *open-mode* (Fig. 2a), the hydraulic resistances at the main channel side and at the control channel side are comparable. Accordingly, the continuous oil phase will flow into both channels. Under these conditions, the discrete water phase requires additional kinetic energy to break the oil 'barrier' (marked with a hollow pink arrow) and penetrate the main channel. Therefore, the water flows into the control channel and is carried away by the continuous oil phase. In *closed-mode* operation (Fig. 2b), the resistance of the control channel suddenly becomes infinitely higher than the main channel. Hence, there is no net flow through the control channel and the incoming water and oil phases are forced to enter the main channel. A more detailed analysis of the force balances at the interface is provided elsewhere.[30]

By utilizing this simple control mechanism only stable droplets of the desired size (from the very first one) can be allowed into the main channel of the chip (where the experiment of interest has been previously hardcoded). The operational method is outlined in Fig. 3 (and Video S3†). In *open-mode*, initial impurities (most normally a chaotic mixture of different phases) can be fully eliminated through the control channel (Fig. 3a(ii) and (iii)). When the stable water stream is introduced, it is sheared by the oil flux at the junction and forms a regular droplet stream that is expelled through the control channel. The desired size of "future" droplets can then be set by simply adjusting the water flow rate without inducing contamination (Fig. 3a(ii) to a(v)). Triggering *closed-mode* results in the water stream receding into the inlet channel and the termination of droplet production (Fig. 3a(v) and a(vi)). The water steam moves forward again and is sheared by the oil in the main channel creating stable droplets of the desired size. Fig. 3b illustrates the high level of monodispersity of the droplets generated by this method (with an area standard deviation of 1.8%). Water stream recession into the water inlet is caused by a certain degree of elasticity inherent to the microfluidic system (due to the use of an elastomeric chip and flexible tubing), which in turn causes a temporal pressure fluctuation. However, as evidenced by the high degree of monodispersity of the formed droplets, this transient instability does not affect droplet production. Pressure-based instabilities can be conveniently analysed and harnessed by equivalent electrical circuit theory.[35] Two analogous electronic circuits corresponding to the microfluidic networks in the two operational modes are presented in Fig. 3c. In analogy to Ohm's law for electrical circuits, the Hagen–Poiseuille law describes the pressure drop in pressure-driven fluid channels at steady state, and can be simplified as,

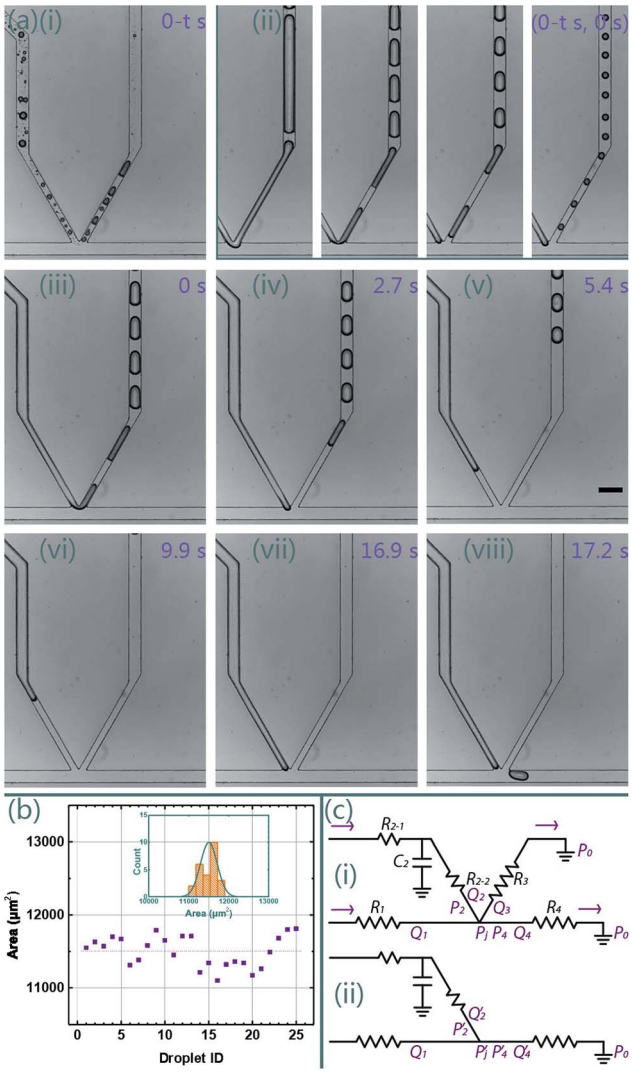

Fig. 3 (a) Sequence of steps used to create stable water droplets from the first one. (i–iii) *Open-mode*. (i) The initial chaotic mixture of phases is eliminated. (ii) Adjusting the water flow rate leads to the desired droplet size at (viii). (iii) When the system has stabilized abandoned droplets are generated in the control channel. (iv–viii) Switch to *closed-mode*. (iv–vii) The water phase stops, recedes and moves forward. (viii) The first targeted droplet in the main channel is generated. Subsequent droplets can be seen in Video S3.† The scale bar is 200 μm. (b) Measurement of droplet areas for the first 25 droplets (area standard deviation = 1.8%). (c) Electrical equivalent circuit models for the two modes. (i) *Open-mode*. (ii) *Closed-mode*.

$$\Delta P = QR \tag{1}$$

here P is the pressure, Q is the volumetric flow-rate and R is the hydraulic resistance. Assuming that oil and water are both incompressible fluids, pressure fluctuations can trigger temporal changes in the channel (and tubing) volumes due to their elasticity. This short-lived transitional behaviour can be treated as an equivalent electric capacitance, *i.e.*

$$Q_t = C\frac{d\Delta P}{dt} \tag{2}$$

where C is the hydrodynamic capacitance and Q_t is the transitional flow-rate. The formal positive directions of Q are marked with arrows in Fig. 3c(i), where a positive value of Q means that flow follows the arrow. In *open-mode* (Fig. 3c(i)), after the system has reached equilibrium, the pressure at the junction, P_j, is equal to P_4, *i.e.*

$$P_j = P_4 \tag{3}$$

$$P_4 = P_o + Q_4R_4 \tag{4}$$

where P_o is the pressure at the outlet of the main channel (*i.e.* atmospheric pressure). Furthermore

$$P_j = P_2 \tag{5}$$

$$Q_1 + Q_2 = Q_3 + Q_4 \tag{6}$$

and using the observation that all the water flow (plus some oil) is taken into the control channel.

$$Q_2 < Q_3 \tag{7}$$

Shortly after closing the control channel (*closed-mode*, Fig. 2c(ii)), all the oil immediately flows through the main channel. Along the main channel (from the oil inlet to the outlet) and for the different channels close to the junction a transient steady state is reached, and it can be assumed that the pressure is constant. Accordingly,

$$P'_j = P'_4 \tag{8}$$

$$P'_4 = P_o + Q'_4R_4 \tag{9}$$

$$Q'_4 = Q_1 \tag{10}$$

$$P'_2 = P_2 \tag{11}$$

Combination of eqn (3)–(11), leads to

$$P'_j - P'_2 = (Q_3 - Q_2)R_4 > 0 \tag{12}$$

which indicates that an increase in pressure at the junction due to control channel closure upsets the local pressure balance, and leads to a temporary recessive flow into the water channel (coupled with a channel/tubing expansion).

By switching between these two modes the device can achieve a 'droplet-on-demand'-like operation (although the exact number of droplets produced is not selected). This function can be extended further to enable clean switching of multiple samples (Fig. 4). To begin with, and by using the protocol discussed above, droplets containing the first aqueous sample are precisely and neatly delivered into the main channel (Fig. 4a–d). To form droplets containing the second sample, the system is reset to *open-mode* (by removing the clip from the tubing). Droplets of the first sample are then eliminated through the control channel (not shown). Subsequently, the world-to-chip interface for the first sample can be disconnected while

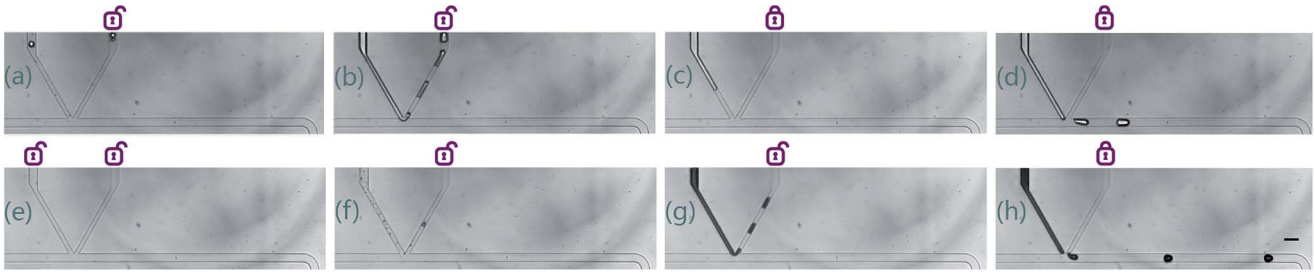

Fig. 4 Images showing clean sample switching. (a–d) Water droplets are generated by the method illustrated in Fig. 3a. (e) By opening the control-tubing and removing the water input tubing, oil refills the entire chip. (f) Connection of the ink input tubing. Initial unwanted impurities are removed until ink droplets are generated in the control channel (g). (h) Closure of the control tubing causes stable ink droplet generation in the main channel. The scale bar is 200 μm.

maintaining the flow of oil that keeps the main channel isolated (Fig. 4e). Next, the world-to-chip interface of the second sample can be connected. Infusion of the second sample is then initiated until, after impurities from the previous sample have been eliminated (Fig. 4f), stable droplets are produced again in the control channel (Fig. 4g). At this point, the system can be switched to *closed-mode* and stable droplets of the second sample of the desired volume are delivered into the main channel (Fig. 4h). A key feature of this simple strategy is that during the whole process not a single unsolicited droplet or

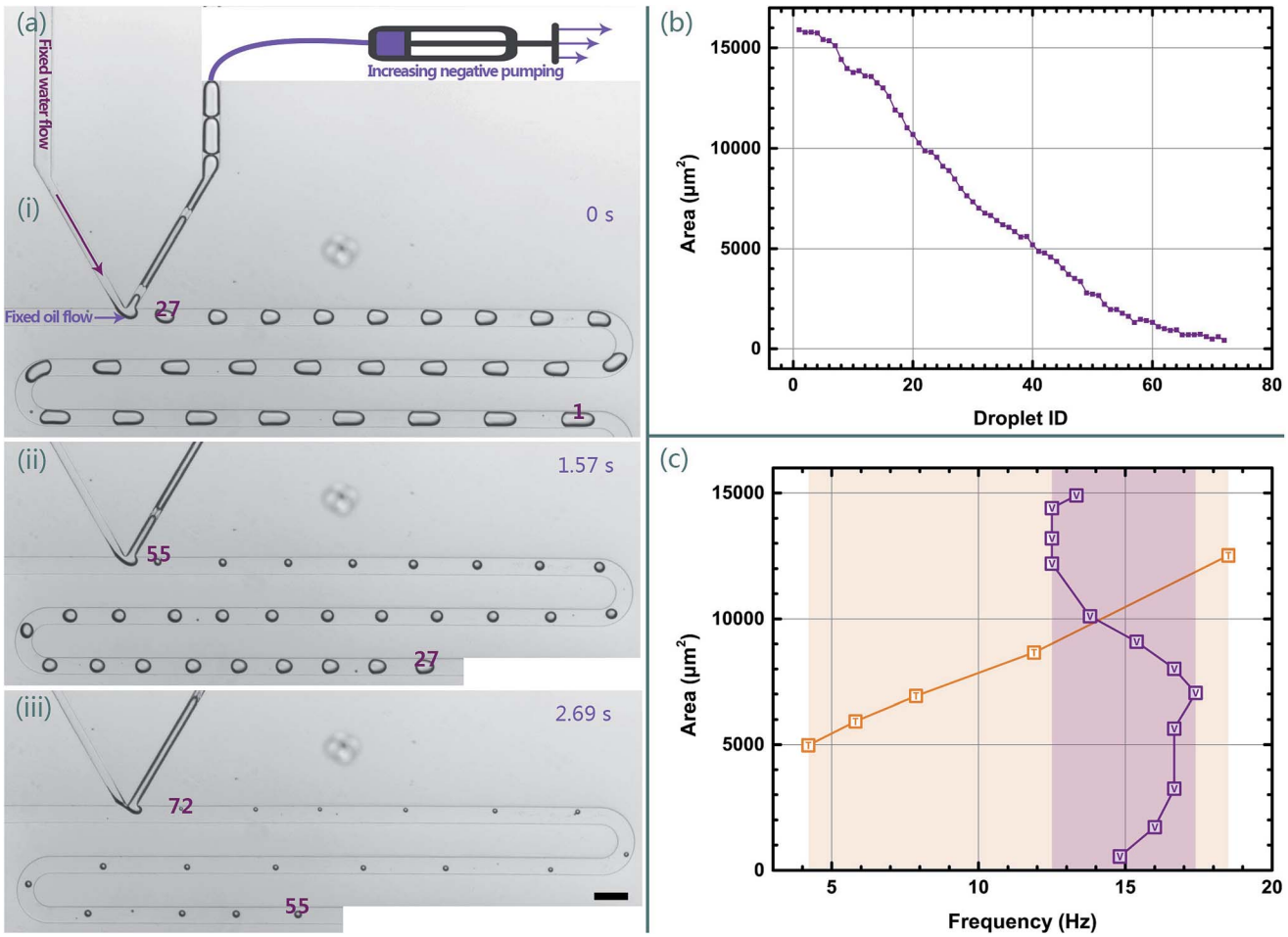

Fig. 5 (a) A droplet size gradient generated by linearly increasing suction at the control channel. Images (ai) to (aiii) display the full sequence of droplet formation (consisting of 72 droplets). Numbers on droplets indicate droplet ID. The scale bar is 200 μm. Small 'satellite' droplets in the pictures originate from oil impurities (see Video S4†). (b) The area of the droplets for (a) is plotted, with the largest 15 910 μm^2 (≈900 pl in volume) and the smallest 416 μm^2 (≈8 pl in volume). (c) Plot for the relationship between droplet generation frequency and size for V and T when oil flow-rates both are 2 $\mu l\ min^{-1}$. The detailed measurement is available in the ESI.†

contaminant pollutes the main channel. Furthermore, the procedure does not require any special skills or equipment to function.

A universal droplet generator with a magic knife

The ability to precisely control the size of the droplets is a key feature of microfluidic emulsion generation. Certain droplet operations are only possible for a limited range of droplet sizes, spacings and frequencies, and especially important for passive droplet manipulations such as fusion[16,36] dilution,[18,37] synchronization,[38] and trapping.[12,22,39] Furthermore, the droplet size is an essential parameter in applications such as bubble logic,[35,40] microgel particle synthesis,[15,41] and studies at the single molecule level (where femtoliter or sub-femtoliter droplets are attractive assaying platforms).[42,43]

With the addition of simple control strategies (such as connecting the control channel to another pump in "withdraw" mode) highly tuneable and precise droplet volumes can be obtained. In the current system, the sharp corner between the control and main channels provides a "knife-like" structure that "cuts" forming droplets and splits them between the two channels. Such a splitting process can be regulated by adjustment of the pressure in the control channel. In essence, the system can behave as an asymmetric, tuneable droplet splitter.[44] To demonstrate the additional functionalities of this system, a sequence of droplets with a size gradient was created (Fig. 5a and b) by linearly increasing suction on the control channel while keeping the flow rates of oil and water constant (at 2 μl min^{-1} and 1 μl min^{-1}, respectively). Although it is possible to produce droplets with size gradients at a conventional T-junction by varying the flow of the discrete phase (Fig. S6†), a much larger range of size gradients is attainable using the V-junction. Specifically, in the current system, the maximum/minimum volume ratio using the V-junction is above 100 while in the T-junction experiment this ratio is less than 2.

Another key attribute of our system is its operational flexibility. When producing droplets using T-junction geometries, the parameters that define the droplet generation process (size, spacing and frequency) are intimately related, *i.e.* it is not possible to modify one without altering another in some way. For example, to produce the smallest possible droplets (65 μm diameter) in a T-junction of comparable dimensions to the current V-junction, the water flow-rate (with an oil flow rate of 2 μl min^{-1}) is decreased to 0.05 μl min^{-1}. Under these conditions, lower frequencies and larger spacings result, which is not the case when using the V-junction (see Fig. S7†). This is primarily due to the different droplet formation mechanisms that apply to each system. Besides the capillary number (which determines the droplet size for the T-junction),[45] the size of droplets at the V-junction is dominated by the splitting effect. A comparison of the relationship between droplet size and generation frequency for an oil flow-rate of 2 μl min^{-1} is provided in Fig. 5c (and Table S3†). Besides the evident capacity of the V-junction to generate smaller droplets, the generation frequency is also independent of the droplet size. Detailed measurements and a discussion of the relationship between spacing and size are provided in the ESI.†

It is also interesting to note that the current design allows the generation of femtoliter-volume droplets. Using the same V-junction (50 μm cross-section), droplet diameters as small as 4.0 ± 0.6 μm (33.5 fl in volume) can be generated along the control channel (which now would act as the "main" channel) in a controllable manner (Fig. 6 and Video S5†). Further geometric optimization and adjustments in the surfactant concentration (such as performed by Yang and co-workers)[46] should permit the direct formation of sub-femtoliter droplets. The V-junction can, therefore, access a larger experimental space for any given droplet-based assay than the traditional T-junction, which suggests its potential as a truly universal droplet generator. Furthermore, its adoption simplifies design factors by eliminating the need to consider the size of the droplet generator, allowing researchers to focus only on the 'downstream' functions.

The return of the droplet: temporal gradient formation

Reagent incubation and temporal control of a given assay are essential steps in most chemical and biological experiments,[12,47] and cell-based screens.[48] Common incubating strategies implemented in microdroplet platforms have traditionally used long winding channels,[23] large open reservoirs,[17] droplet-trapping arrays for on-chip incubation[49] or off-chip storage (*e.g.* in Eppendorf tubes).[48,50] The temporal control of droplets (*i.e.* residence times) is traditionally achieved by simply assaying the droplets at different positions along the channel length in the direction of flow. This is advantageous if a large number of droplets are available (meaning that many can be overlooked while the system is moved to a new measurement position). However, for small numbers of droplets (such as those obtained from a very small sample volume), it is beneficial to assay all available droplets, which requires that each unit is associated with a specific residence time. In this context, the V-junction

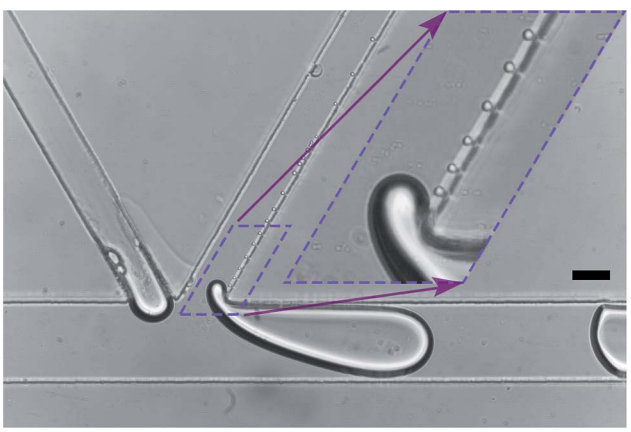

Fig. 6 Image showing the formation of small droplets by application of a slight negative pressure at the control channel. Such droplets are obtained by splitting the forming droplet into two unequal daughter droplets. Smaller droplets, with a size of 4.0 ± 0.6 μm in diameter, are conveyed along the control channel. The area marked with a purple dashed box is magnified to highlight these small droplets. The scale bar is 50 μm. The corresponding video is shown in Video S5.†

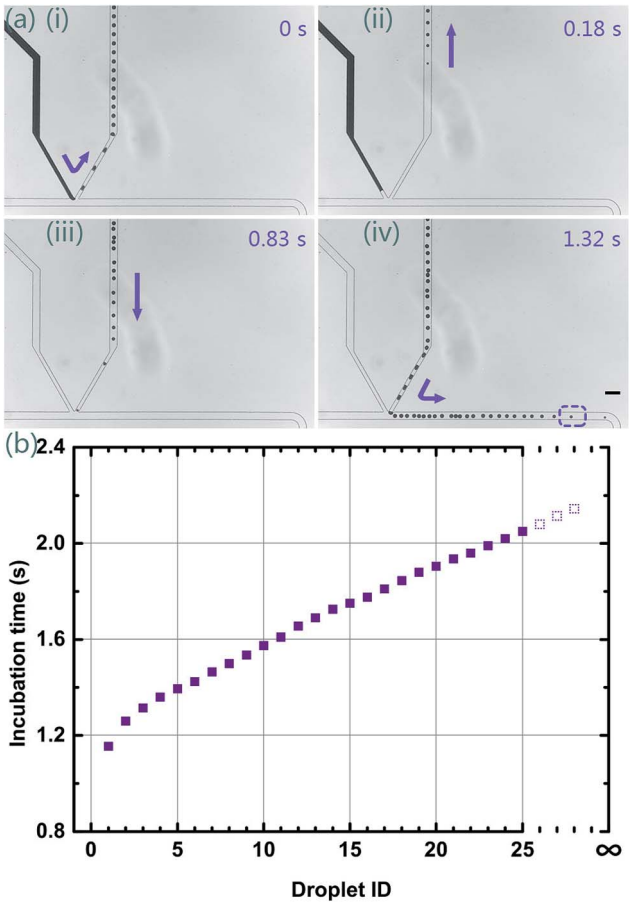

Fig. 7 (a) Generation of residence time gradients. (i) Droplets are generated in the control channel under negative pressure. (ii) Water infusion is stopped. (iii) Subsequently, a positive pressure is applied on the control channel: droplets come back and enter the main channel in a reversed sequence (iv). (b) The residence time for droplets in the sequence (*i.e.* temporal gradient) is obtained at the area marked with the dashed box in the image (a(iv)). The scale bar is 200 μm. The associated Video S6† is available.

can conveniently perform these tasks without the need for any additional steps or control architectures, as illustrated in Fig. 7 and Video S6.† First, droplets are generated in the control channel obtaining a droplet sequence (Fig. 7a(i)). The flow of the discrete phase is then stopped (Fig. 7a(ii)) and the droplets in the control channel are pushed back into the main channel (Fig. 7a(iv)), effectively reversing the droplet sequence. If a fixed detection window is set up in the main channel (marked by a purple dashed box in Fig. 7a(iv)), droplets crossing this section display a gradient of increasing incubation or residence time (Fig. 7b). This simple method allows performance of experiments where incubation or temporal gradients of the droplet-processed sample (which are much more complex to achieve) constitute analytical dimensions of interest.

Conclusions

We have presented a novel component for microdroplet generation, which we termed as the V-junction. The V-junction matches the simplicity of operation of regular T-junction formats whilst enabling a wider range of functionalities that are normally only attainable when using robotic, droplet-on-demand systems. Manufacturing of the V-junction does not add extra complexity to the fabrication process and only requires the use of an additional pumping source. The V-junction can complete additional tasks such as the formation of monodisperse droplets of desired size from the very first one, clean switching of samples and the production of a large range of droplet sizes. It is capable of creating a stable droplet sequence with a wide combination of sizes, spacings and frequencies, providing a more universal generation method that can accommodate a broader range of downstream experiments. Furthermore, the system allows the creation of femtoliter-volume droplets and the performance of complex tasks such as on-chip incubation and the formation of droplets with temporal gradients. We hope that the component will be readily transferrable to any biology and chemistry laboratory willing to implement droplet-based experimentation.

Acknowledgements

The authors acknowledge the provision of a China Scholarship Council fellowship for YD, technical support from Dr Stavros Stavrakis and partial support from ETH Zürich and the Global Research Laboratory Program of the National Research Foundation of Korea (grant number K20904000004-11A0500-00410).

Notes and references

1 J. D. Ramsey, S. C. Jacobson, C. T. Culbertson and J. M. Ramsey, *Anal. Chem.*, 2003, **75**, 3758–3764.
2 M. T. Guo, A. Rotem, J. A. Heyman and D. A. Weitz, *Lab Chip*, 2012, **12**, 2146–2155.
3 J. S. Marcus, W. F. Anderson and S. R. Quake, *Anal. Chem.*, 2006, **78**, 3084–3089.
4 H. Song, J. D. Tice and R. F. Ismagilov, *Angew. Chem., Int. Ed.*, 2003, **42**, 768–772.
5 T. M. Squires and S. R. Quake, *Rev. Mod. Phys.*, 2005, **77**, 977–1026.
6 D. Erickson, D. Sinton and D. Li, *Lab Chip*, 2003, **3**, 141–149.
7 C. J. Easley, J. M. Karlinsey, J. M. Bienvenue, L. A. Legendre, M. G. Roper, S. H. Feldman, M. A. Hughes, E. L. Hewlett, T. J. Merkel, J. P. Ferrance and J. P. Landers, *Proc. Natl. Acad. Sci. U. S. A.*, 2006, **103**, 19272–19277.
8 S.-Y. Teh, R. Lin, L.-H. Hung and A. P. Lee, *Lab Chip*, 2008, **8**, 198–220.
9 H. N. Joensson and H. Andersson Svahn, *Angew. Chem., Int. Ed.*, 2012, **51**, 12176–12192.
10 T. Thorsen, R. W. Roberts, F. H. Arnold and S. R. Quake, *Phys. Rev. Lett.*, 2001, **86**, 4163–4166.
11 S. L. Anna, N. Bontoux and H. A. Stone, *Appl. Phys. Lett.*, 2003, **82**, 364–366.
12 A. Huebner, D. Bratton, G. Whyte, M. Yang, A. J. deMello, C. Abell and F. Hollfelder, *Lab Chip*, 2009, **9**, 692–698.
13 J. D. Tice, H. Song, A. D. Lyon and R. F. Ismagilov, *Langmuir*, 2003, **19**, 9127–9133.

14 L. Frenz, K. Blank, E. Brouzes and A. D. Griffiths, *Lab Chip*, 2009, **9**, 1344–1348.
15 Y. Wang, E. Tumarkin, D. Velasco, M. Abolhasani, W. Lau and E. Kumacheva, *Lab Chip*, 2013, **13**, 2547–2553.
16 X. Niu, S. Gulati, J. B. Edel and A. J. deMello, *Lab Chip*, 2008, **8**, 1837.
17 A. C. Hatch, J. S. Fisher, A. R. Tovar, A. T. Hsieh, R. Lin, S. L. Pentoney, D. L. Yang and A. P. Lee, *Lab Chip*, 2011, **11**, 3838–3845.
18 X. Niu, F. Gielen, J. B. Edel and A. J. deMello, *Nat. Chem.*, 2011, **3**, 437–442.
19 M. A. Cartas-Ayala, M. Raafat and R. Karnik, *Small*, 2013, **9**, 375–381.
20 N.-N. Deng, S.-X. Sun, W. Wang, X.-J. Ju, R. Xie and L.-Y. Chu, *Lab Chip*, 2013, **13**, 3653–3657.
21 Y. Bai, X. He, D. Liu, S. N. Patil, D. Bratton, A. Huebner, F. Hollfelder, C. Abell and W. T. S. Huck, *Lab Chip*, 2010, **10**, 1281–1285.
22 X. C. i Solvas, V. Turek, T. Prodromakis and J. B. Edel, *Lab Chip*, 2012, **12**, 4049–4054.
23 Y. Schaerli, R. C. Wootton, T. Robinson, V. Stein, C. Dunsby, M. A. A. Neil, P. M. W. French, A. J. deMello, C. Abell and F. Hollfelder, *Anal. Chem.*, 2009, **81**, 302–306.
24 R. Seemann, M. Brinkmann, T. Pfohl and S. Herminghaus, *Rep. Prog. Phys.*, 2012, **75**, 016601.
25 G. F. Christopher and S. L. Anna, *J. Phys. D: Appl. Phys.*, 2007, **40**, R319.
26 S. Zeng, B. Li, X. Su, J. Qin and B. Lin, *Lab Chip*, 2009, **9**, 1340–1343.
27 Y. Zeng, M. Shin and T. Wang, *Lab Chip*, 2012, **13**, 267–273.
28 H. Zec, T. D. Rane and T.-H. Wang, *Lab Chip*, 2012, **12**, 3055–3062.
29 F. Gielen, L. van Vliet, B. T. Koprowski, S. R. A. Devenish, M. Fischlechner, J. B. Edel, X. Niu, A. J. deMello and F. Hollfelder, *Anal. Chem.*, 2013, **85**, 4761–4769.
30 R. Lin, J. S. Fisher, M. G. Simon and A. P. Lee, *Biomicrofluidics*, 2012, **6**, 024103.
31 Y. Xia and G. M. Whitesides, *Angew. Chem., Int. Ed.*, 1998, **37**, 550–575.
32 D. T. Eddington, J. P. Puccinelli and D. J. Beebe, *Sens. Actuators, B*, 2006, **114**, 170–172.
33 A. S. Basu, *Lab Chip*, 2013, **13**, 1892–1901.
34 https://sites.google.com/site/qingzongtseng/piv.
35 K. W. Oh, K. Lee, B. Ahn and E. P. Furlani, *Lab Chip*, 2012, **12**, 515–545.
36 N. Bremond, A. R. Thiam and J. Bibette, *Phys. Rev. Lett.*, 2008, **100**, 024501.
37 P. M. Korczyk, L. Derzsi, S. Jakiela and P. Garstecki, *Lab Chip*, 2013, **13**, 4096–4102.
38 B. Ahn, K. Lee, H. Lee, R. Panchapakesan and K. W. Oh, *Lab Chip*, 2011, **11**, 3956–3962.
39 S. S. Bithi and S. A. Vanapalli, *Biomicrofluidics*, 2010, **4**, 044110.
40 M. Prakash and N. Gershenfeld, *Science*, 2007, **315**, 832–835.
41 S. Xu, Z. Nie, M. Seo, P. Lewis, E. Kumacheva, H. A. Stone, P. Garstecki, D. B. Weibel, I. Gitlin and G. M. Whitesides, *Angew. Chem.*, 2004, **117**, 734–738.
42 J. Shim, R. T. Ranasinghe, C. A. Smith, S. M. Ibrahim, F. Hollfelder, W. T. S. Huck, D. Klenerman and C. Abell, *ACS Nano*, 2013, **7**, 5955–5964.
43 R. Arayanarakool, L. Shui, S. W. M. Kengen, A. van den Berg and J. C. T. Eijkel, *Lab Chip*, 2013, **13**, 1955–1962.
44 B. Verbruggen, T. Tóth, Y. T. Atalay, F. Ceyssens, P. Verboven, R. Puers, B. Nicolai and J. Lammertyn, *Microfluid. Nanofluid.*, 2013, **15**, 243–252.
45 P. Garstecki, M. J. Fuerstman, H. A. Stone and G. M. Whitesides, *Lab Chip*, 2006, **6**, 437.
46 Y.-J. Yang, X. Feng, N. Xu, D.-W. Pang and Z.-L. Zhang, *Appl. Phys. Lett.*, 2013, **102**, 123502.
47 H. Song, D. L. Chen and R. F. Ismagilov, *Angew. Chem., Int. Ed.*, 2006, **45**, 7336–7356.
48 E. Brouzes, M. Medkova, N. Savenelli, D. Marran, M. Twardowski, J. B. Hutchison, J. M. Rothberg, D. R. Link, N. Perrimon and M. L. Samuels, *Proc. Natl. Acad. Sci. U. S. A.*, 2009, **106**, 14195–14200.
49 R. R. Pompano, W. Liu, W. Du and R. F. Ismagilov, *Annu. Rev. Anal. Chem.*, 2011, **4**, 59–81.
50 M. Lee, J. W. Collins, D. M. Aubrecht, R. A. Sperling, L. Solomon, J.-W. Ha, G.-R. Yi, D. A. Weitz and V. N. Manoharan, *Lab Chip*, 2014, **14**, 509–513.